THE JOURNAL OF BIOLOGICAL CHEMISTRY VOL. 288, NO. 27, pp. 19773–19784, July 5, 2013

Enhanced Phosphatidylinositol 3-kinase (PI3K)/Akt Signaling Has Pleiotropic Targets in Hippocampal Neurons Exposed to Iron-induced Oxidative Stress*

Received for publication, January 29, 2013, and in revised form, May 7, 2013 Published, JBC Papers in Press, May 16, 2013, DOI 10.1074/jbc.M113.457622

Romina María Uranga[‡§¶], **Sebastián Katz**[§¶], **and Gabriela Alejandra Salvador**[‡§¶1]

From the [‡]*Instituto de Investigaciones Bioquímicas de Bahía Blanca,* [§]*Universidad Nacional del Sur, and* [¶]*Consejo Nacional de Investigaciones Científicas y Técnicas, 8000 Bahía Blanca, Argentina*

Background: The PI3K/Akt pathway is activated upon oxidative stress.
Results: The PI3K/Akt pathway partially protects the neuron against cellular oxidant generation via FoxO3a phosphorylation.
Conclusion: The PI3K/Akt pathway plays a pleiotropic protective role under oxidative stress.
Significance: This pathway could be used as a therapeutic target in oxidative stress-related disorders.

The PI3K/Akt pathway is a key component in synaptic plasticity and neuronal survival. The aim of this work was to investigate the participation of the PI3K/Akt pathway and its outcome on different molecular targets such as glycogen synthase kinase 3β (GSK3β) and Forkhead box-O (FoxO) transcription factors during mild oxidative stress triggered by iron overload. The exposure of mouse hippocampal neurons (HT22) to different concentrations of Fe^{2+} (25–200 μM) for 24 h led us to define a mild oxidative injury status (50 μM Fe^{2+}) in which cell morphology showed changes typical of neuronal damage with increased lipid peroxidation and cellular oxidant levels but no alteration of cellular viability. There was a simultaneous increase in both Akt and GSK3β phosphorylation. Levels of phospho-FoxO3a (inactive form) increased in the cytosolic fraction of cells treated with iron in a PI3K-dependent manner. Moreover, PI3K and Akt translocated to the nucleus in response to oxidative stress. Iron-overloaded cells harboring a constitutively active form of Akt showed decreased oxidants levels. Indeed, GSH synthesis under oxidative stress conditions was regulated by activated Akt. Our results show that activation of the PI3K/Akt pathway during iron-induced neurotoxicity regulates multiple targets such as GSK3β, FoxO transcriptional activity, and glutathione metabolism, thus modulating the neuronal response to oxidative stress.

Iron-induced oxidative stress is a hallmark of neurodegenerative disorders such as Alzheimer's disease (AD)[2] and Parkinson's disease (1, 2). This redox milieu in which neurons are immersed becomes extremely hostile, enhancing neurodegeneration processes and triggering multiple and opposing cellular responses. The precise molecular targets providing neuronal resistance to oxidative stress and the manner in which neurons determine their final fate of survival or death are still to be elucidated.

In this connection, the serine-threonine kinase Akt has been studied extensively because of its participation in cellular outcome. Akt is the main downstream effector of PI3K (3, 4). Its activation is initiated by membrane recruitment via interaction of its pleckstrin homology domain with phosphatidylinositol 3,4,5-trisphosphate synthesized by PI3K from phosphatidylinositol 4,5-bisphosphate. After membrane anchoring, Akt is phosphorylated sequentially by phosphoinositide-dependent kinase 1 (PDK-1) at threonine 308 and by the mammalian target of rapamycin complex 2 (mTORC2) at serine 473 (5). Upon phosphorylation, Akt translocates from the plasma membrane to intracellular compartments, including the cytoplasm and nucleus, where it phosphorylates a variety of substrates (6). One of these substrates is glycogen synthase kinase 3β (GSK3β), which is inhibited through phosphorylation at serine 9 by Akt (3). GSK3β activity is involved in neuronal cell death, and cumulative evidence demonstrates the role of GSK3β inhibitors in neuroprotection (7). *In vivo* models overexpressing GSK3β in the brain show signs of neurodegeneration and spatial learning deficits (8). In addition, the decrease in Akt activity and the increase in GSK3β activity have been described in cells from familial AD patients that contain mutated presenilin1/2 (9).

Another target lying downstream of PI3K/Akt signaling is the class O of forkhead box (FoxO) transcription factors. The FoxO family binds to the Forkhead response element and increases the expression of proapoptotic genes (10). The transcriptional activity of FoxO is dependent on the phosphorylation of three key residues (threonine 24, serine 256, and serine 319) by Akt. The phosphorylation state of FoxO governs its

* This work was supported by Universidad Nacional del Sur Grant PGI 24/B179), by Agencia Nacional de Promoción Científica y Tecnológica (ANPCyT) Grant PICT-2010-0936), by Consejo Nacional de Investigaciones Científicas y Técnicas (CONICET) Grant PIP 11220090100687), and by the Fundación Florencio Fiorini.

[1] To whom correspondence should be addressed: Instituto de Investigaciones Bioquímicas de Bahía Blanca, La Carrindanga Km 7, 8000 Bahía Blanca, Buenos Aires, Argentina. Tel.: 54-291-4861201; Fax: 54-291-4861200; E-mail: salvador@criba.edu.ar.

[2] The abbreviations used are: AD, Alzheimer's disease; FoxO, Forkhead box O; SOD, superoxide dismutase; Aβ, amyloid-beta peptide; DCDCDHF, 2′,7′-dichlorofluorescein diacetate; LY294002, 2-(4-morpholinyl)-8-phenyl-1(4H)-benzopyran-4-one hydrochloride; MTT, 3-(4,5-dimethylthiazol-2-yl)-2,5-diphenyltetrazolium bromide; γ-GCSc, γ-glutamylcysteine synthetase catalytic subunit; PTEN, phosphatase and tensin homolog; ANOVA, analysis of variance; ROS, reactive oxygen species; SirT, sirtuin; TBARS, thiobarbituric acid reactive substances.

subcellular localization (11). Although the triple-phosphorylated form is exported from the nucleus and retained in the cytoplasm in a Crm-1- and 14-3-3-dependent manner, the non-phosphorylated form resides in the nucleus and is capable of transcribing target apoptotic genes (12). Thus, FoxO transcriptional activity is essential in programmed cell death during development but has also been implicated in the initiation of apoptosis during neuronal injury, as in the case of neurodegenerative disorders in the mature nervous system (13, 14).

One opposite and unexpected role for Akt has been described by Nogueira *et al.* (15). They demonstrated that strongly activated Akt increases oxidative stress levels and makes the cell more susceptible to oxidative injury. This increase in pro-oxidant conditions could be caused by the Akt-dependent up-regulation of oxidative phosphorylation and oxygen consumption. In addition, hyperactivated Akt could lead to a sustained inhibition of FoxO transcription factors, particularly FoxO3a, which normally up-regulates the expression of antioxidant proteins such as superoxide dismutase (SOD) 2, catalase, and sestrins (16, 17). These intriguing findings relating to the ability of Akt to increase reactive oxygen species through the down-regulation of antioxidant defenses could be a double-edged sword and appear to be strictly related to the extent and time-lapse of Akt activation. In cancer cells, this ability could be exploited by using oxidant therapies, but in neurons it could lead to lethal damage under brain oxidative conditions, as it is the scenario of AD and Parkinson's disease. Thus, the mechanism of Akt participation in neuronal oxidative injury remains puzzling and largely unclear.

In previous work from our laboratory, we demonstrated that iron-induced oxidative damage activates the PI3K/Akt pathway in synaptic terminals, GSK3β being one of the main downstream effectors (18, 19). We also demonstrated that synaptic Akt and ERK 1/2 signaling were differentially activated by the presence of amyloid β peptide (Aβ) and iron overload (20). However, the role of synaptic Akt activation in neuronal fate can only be fully understood if it is studied in the whole neuron. In view of the above, the aim of this study has been to describe the role of PI3K/Akt activation during iron-induced oxidative injury in hippocampal neurons. Our attention has been focused mainly on two main targets of PI3K/Akt-FoxO3a and GSK3β, their involvement in the response to oxidative injury and, ultimately, the determination of neuronal fate.

EXPERIMENTAL PROCEDURES

Cell Culture, Chemicals, and Treatments—HT22 cells, a stable murine hippocampal cell line, were used for the experiments. Cells were maintained in DMEM supplemented with 10% FBS (Natocor, Argentina), 100 units/ml penicillin, 100 μg/ml streptomycin, and 0.25 μg/ml amphotericin B at 37 °C under 5% CO_2. For all experiments, cells were grown to 80–90% confluence. Transfection was carried out with Lipofectamine 2000 (Invitrogen). Ferrous sulfate (J. T. Baker, catalog no. 2070-01) was purchased in EMD Millipore (Millipore, Bedford, MA). Inhibitor IV (catalog no. sc-203809) was purchased from Santa Cruz Biotechnology (Santa Cruz, CA). 2′,7′-Dichlorofluorescein diacetate (DCDCDHF, catalog no. D6883), 2-(4-morpholinyl)-8-phenyl-1(4H)-benzopyran-4-one hydrochloride (LY294002, catalog no. L9908), lithium chloride (catalog no. L9650), 3-(4,5-dimethylthiazol-2-yl)-2,5-diphenyltetrazolium bromide (MTT, catalog no. M2128), and DAPI (catalog no. D9542) were purchased from Sigma Aldrich (St. Louis, MO). Fe^{2+} treatments were carried out in serum-free medium. Treatments with LY294002, lithium (Li^+), and inhibitor IV were performed as follows. Medium was removed and replaced by serum-free medium. Inhibitors were then added to the desired final concentration (controls received vehicle alone). After 30 min, Fe^{2+} was added, and cells were incubated under these conditions for 24 h.

Antibodies—Antibodies against catalase (catalog no. sc-34285), SOD1 (catalog no. sc-11407), SOD2 (catalog no. sc-30080), β-actin (catalog no. sc-47778), γ-GCSc (catalog no. sc-22755), and human NAP-related protein (catalog no. sc-32301) were purchased from Santa Cruz Biotechnology. Antibodies against phospho-Ser-473-Akt (catalog no. cs9271), Akt (catalog no. cs9272), phospho-Ser-9-GSK3β (catalog no. cs9336), GSK3β (catalog no. cs9332), PTEN (catalog no. cs9556), phospho-Ser-253-FoxO3a (catalog no. cs9466), FoxO3a (catalog no. cs2497), and sirtuin 3 (catalog no. cs2627) were purchased from Cell Signaling Technology (Beverly, MA). Antibody against MAPK/ERK kinase (catalog no. SAB4502404) was purchased from Sigma Aldrich. Antibody against PI3K (catalog no. 06-497) was purchased from Upstate/Millipore (Temecula, CA). Antibody against HA was purchased from BAbCo (Richmond, CA). Cy-2-conjugated secondary antibodies were from Jackson ImmunoResearch (West Grove, PA).

Plasmids—Expression plasmids, including pCMV6-Myr-Akt-HA (Myr-Akt), pECE-HA-FoxO3a WT (FoxO3a-WT), and pECE-HA-FoxO3a TM (FoxO3a-TM), were gifts from Dr. Alex Toker (Beth Israel Deaconess Medical Center, Harvard Medical School).

Assessment of Cell Viability—Cell viability was assessed by MTT reduction assay. MTT is a water-soluble tetrazolium salt that is reduced by metabolically viable cells to a colored, water-insoluble formazan salt. After treatments, MTT (5 mg/ml) was added to the cell culture medium at a final concentration of 0.5 mg/ml. After incubating the plates for 2 h at 37 °C in a 5% CO_2 atmosphere, the assay was stopped, and the MTT-containing medium was replaced with solubilization buffer (20% SDS (pH 4.7)). The extent of MTT reduction was measured spectrophotometrically at 570 nm. Results are expressed as a percentage of the control.

Determination of Lipid Peroxidation—Lipid peroxidation was determined by thiobarbituric acid reactive substances (TBARS) assay, which involves derivatization of malondialdehyde with thiobarbituric acid to produce a pink product that is quantified in a UV-visible spectrophotometer. Briefly, after treatments, cells were scraped off into 200 μl of ice-cold water and mixed with 0.5 ml of 30% TCA. Then, 50 μl of 5 N HCl and 0.5 ml of 0.75% thiobarbituric acid were added. Tubes were capped, the mixtures were heated at 100 °C for 15 min in a boiling water bath, and the samples were centrifuged at 1000 × *g* for 10 min. TBARS were measured spectrophotometrically in the supernatant at 535 nm. Results are expressed as a percentage of the control.

Determination of Cell Oxidant Levels—Cell oxidative stress was evaluated using DCDCDHF. This probe can cross the membrane, and, after oxidation, it is converted into a fluorescent compound. After the corresponding treatments, the medium was discarded, and complex medium containing 10 μM DCDCDHF (Molecular Probes, Eugene, OR) was added. After 30 min of incubation at 37 °C, the medium was removed, and cells were rinsed three times with PBS and then either imaged with an epifluorescence microscope or lysed in a buffer containing PBS and 1% Nonidet P-40. Fluorescence in the lysates ($\lambda_{ex} = 538$, $\lambda_{em} = 590$) was measured in an SLM model 4800 fluorimeter (SLM Instruments, Urbana, IL). Results are expressed as arbitrary units.

Cytoplasmic and Nuclear fractionation with Nonidet P-40 Detergent-containing Buffer—Nuclear and cytosolic fractions were isolated as described previously (21, 22). After treatments, the medium was discarded, and cells were rinsed with PBS and scraped. After centrifugation at 800 × *g* for 10 min, the pellet (10×10^6 cells) was resuspended in 100 μl of buffer A (10 mM HEPES (pH 7.9), 1.5 mM $MgCl_2$, 10 mM KCl, 0.5 mM DTT, 0.1% Nonidet P-40, 2 μg/μl leupeptin, 1 μg/μl aprotinin, 1 μg/μl pepstatin), incubated for 10 min at 4°C, and centrifuged for 2 min at 12,000 × *g*. The supernatant (cytosolic fraction) was removed, and the nuclear pellet was resuspended in 40 μl of buffer B (10 mM HEPES (pH 7.9), 1.5 mM $MgCl_2$, 420 mM NaCl, 0.5 mM DTT, 0.2 mM EDTA, 25% glycerol, 0.5 mM PMSF, 2 μg/ml leupeptin, 1 μg/ml aprotinin, 1 μg/ml pepstatin). Samples were incubated for 20 min at 4°C and centrifuged at 10,000 × *g* for 15 min at 4°C. Protein concentration was determined by the method of Bradford (23), and samples were stored at −20°C until used for Western blot analyses.

Western Blot Analysis—For the preparation of total cell extracts, cells (10×10^6 cells) were rinsed with PBS, scraped and centrifuged. The pellet was rinsed with PBS and resuspended in 200 μl of a buffer containing 50 mM Tris (pH 7.5), 150 mM NaCl, 0.1% Triton X-100, 1% Nonidet P-40, 2 mM EDTA, 2 mM EGTA, 50 mM NaF, 2 mM β-glycerophosphate, 1 mM Na_3VO_4, 10 μg/ml leupeptin, 5 μg/ml aprotinin, 1 μg/ml pepstatin, 0.5 mM PMSF, and 0.5 mM DTT. Samples were exposed to one cycle of freezing and thawing, incubated at 4 °C for 30 min, and centrifuged at 15,000 × *g* for 30 min. The supernatant was decanted, and the protein concentration was measured (23). Aliquots of total, nuclear, or cytosolic fractions containing 25–50 μg of protein were separated by reducing 7–12.5% polyacrylamide gel electrophoresis and electroblotted to polyvinylidene difluoride membranes (Millipore). Molecular weight standards (Spectra™ multicolor broad-range protein ladder, Thermo Scientific) were run simultaneously. Membranes were blocked with 5% nonfat dry milk in TBS-T buffer (20 mM Tris-HCl (pH 7.4), 100 mM NaCl, and 0.1% (w/v) Tween 20) for 2 h at room temperature and then incubated with primary antibodies (anti-phospho-Ser-473-Akt, anti-Akt, anti-γ-GCSc, anti-phospho-Ser-9-GSK3β, anti-GSK3β, anti-PTEN, anti-phospho-Ser-253-FoxO3a, anti-FoxO3a, anti-phospho-Ser-256-FoxO1, anti- MAPK/ERK kinase, anti-PI3K, anti-catalase, anti-SOD1, anti-SOD2, anti-β actin, and anti- human NAP-related protein (1:1000) overnight at 4 °C), washed three times with TBS-T, and then exposed to the appropriate HRP-conjugated secondary antibody for 1 h at room temperature. Membranes were again washed three times with TBS-T, and immunoreactive bands were detected by ECL (GE Healthcare) using standard x-ray film (Kodak X-OMAT AR, GE Healthcare). Immunoreactive bands were quantified using image analysis software (ImageJ, a freely available application in the public domain for image analysis and processing developed and maintained by Wayne Rasband at the Research Services Branch, National Institute of Mental Health).

Determination of GSH Levels—GSH content from total cell extracts was determined by using a spectrophotometric assay method that involves oxidation of GSH by the sulfhydryl reagent 5,5′-dithio-bis(2-nitrobenzoic acid) to form the yellow derivative 5′-thio-2-nitrobenzoic acid, measurable at 412 nm.

Immunofluorescence Microscopy—HT22 cells were grown onto glass coverslips, and the growing medium was replaced by serum-free medium. After treatment with 50 μM Fe^{2+} for 24 h, the cells were fixed with precooled methanol for 10 min at −20 °C, followed by two washes in PBS. For the immunostaining, the nonspecific sites were blocked with 5% BSA in PBS at room temperature for 30 min. Cells were incubated with the appropriate primary antibody (1:50 in PBS, 2% BSA, 1 h at room temperature). After three washes with PBS, cells were incubated with Cy-2-conjugated secondary antibody (1:200, 1 h, room temperature) and DAPI or TO-PRO for nuclear staining. After washing with PBS at room temperature for 10 min, coverslips were mounted, and slides were viewed with a Nikon Eclipse Ti-S fluorescence microscope or a Leica TCS SP2 AOBS confocal laser microscope.

Statistical Analysis—Quantitative results were expressed as the means ± S.E. of measurement and analyzed by MTT reduction, TBARS assay, cell oxidant levels, Akt, and GSK3β phosphorylation. PI3K, Akt, GSK3β, and PTEN subcellular redistribution were analyzed by ANOVA to determine group differences, followed by Tukey's post hoc analysis to determine specific differences between conditions. Cell oxidant levels in overexpression experiments were analyzed with two-way, repeated-measures ANOVA to determine the main effects of protein overexpression and treatments, followed by Tukey's post hoc comparisons to determine differences between Fe^{2+} and the control condition and also differences between the overexpressed proteins. Cell oxidant levels in Fig. 1*D* and catalase, SOD1, and SOD2 expression were analyzed by Student's *t* test. Statistical significance for all analyses was accepted at $p < 0.05$. The Western blots shown are representative of at least three analyses performed on samples from at least three separate experiments.

RESULTS

Cellular Effects of Fe^{2+}-induced Oxidative Stress—We have previously characterized an iron-induced oxidative stress model in cerebral cortex synaptic endings (18, 19). We have also described the activation of the PI3K/Akt pathway in synaptic endings exposed to iron-induced oxidative injury (19). In this report, we have moved to a neuronal model to completely characterize the role of PI3K/Akt activation during neuronal iron-induced oxidative stress. For this purpose, murine hippocampal neurons, HT22 cells, were exposed to increasing Fe^{2+} concen-

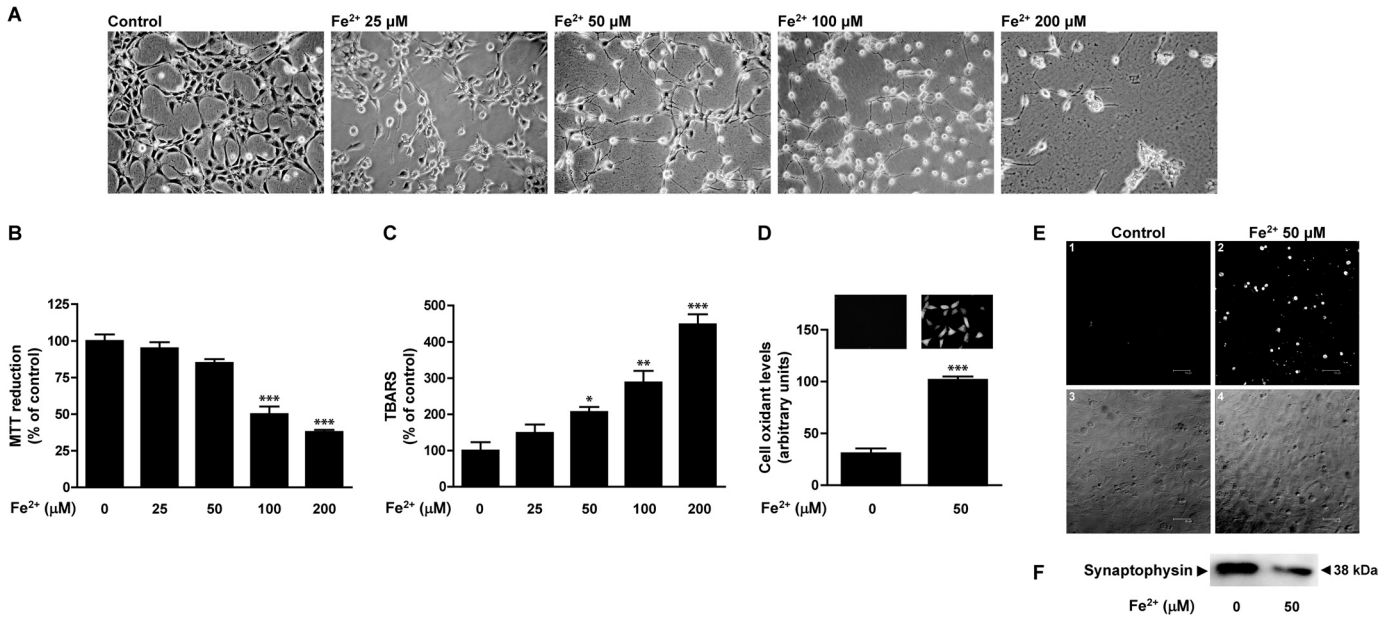

FIGURE 1. **Characterization of the oxidative stress status in HT22 cells after treatments.** *A*, photomicrographs of the cells exposed to Fe^{2+} (0–200 μM). *B*, MTT reduction assay. Cells were treated with Fe^{2+} (0–200 μM) or its vehicle for 24 h, and cell viability was assessed as described under "Experimental Procedures." Results are expressed as a percentage of the control and represent mean ± S.E. ($n = 3$–5). ***, $p < 0.001$ for each condition with respect to the control; one-way ANOVA and Tukey's post hoc test. *C*, TBARS assay. Cells were exposed to Fe^{2+} (0–200 μM) or its vehicle for 24 h, and lipid peroxidation was studied as described under "Experimental Procedures." Results are expressed as a percentage of the control and represent mean ± S.E. ($n = 3$–4). *, $p < 0.05$; **, $p < 0.01$; ***, $p < 0.001$ for each condition with respect to the control; one-way ANOVA and Tukey's post hoc test. *D* and *E*, determination of cellular oxidant levels. Cells were treated with 50 μM Fe^{2+} for 24 h and then incubated in the presence of 10 μM DCDCDHF as described under "Experimental Procedures." Cellular oxidant levels were quantified by spectrofluorometry (*D*) and imaged with an epifluorescence microscope (*E*, *1* and *2*). *3* and *4* in *E* are differential interference contrast images of *1* and *2*, respectively. The results in *D* are expressed as arbitrary units and represent the mean ± S.E. ($n = 3$). ***, $p < 0.001$ with respect to the control; Student's *t* test. The micrographs shown in *E* are representative of at least three analyses performed on samples from at least three separate experiments. *F*, synaptic marker expression. After the exposure to Fe^{2+} 50 μM, cell lysates were prepared for Western blot studies. Synaptophysin expression is shown in a representative blot of three different studies.

trations (25, 50, 100, and 200 μM) for 24 h. Control conditions were also assessed, replacing Fe^{2+} with an equal volume of water (vehicle). To determine the extent of neuronal injury, cell morphology and viability and lipid peroxidation levels were evaluated. As shown in Fig. 1*A*, exposure to the metal ion caused evident morphological alterations typical of neuronal damage (cytoplasmic retraction, rounding of the cell bodies, and diminution in the number of neuronal projections) that were found to be iron concentration-dependent. Cell viability, assessed by MTT reduction assay, was found to be diminished significantly only in the presence of the two highest concentrations of iron assayed (50 and 62% lower than the control condition for 100 and 200 μM, respectively, Fig. 1*B*) where neuronal morphology was extremely altered. Lipid peroxidation levels, evaluated by TBARS assay, were found to be increased significantly by iron concentrations of 50 μM or higher (107%, 189%, and 349% higher than the control for 50, 100, and 200 μM, respectively, Fig. 1*C*). Because 50 μM Fe^{2+} was found to be the lowest concentration of the metal ion capable of causing noticeable morphological changes, with a slight but significant increase in lipid peroxidation but no significant mitochondrial dysfunction and death, we next assessed the levels of cellular oxidants generated by the exposure to this concentration of iron. A very significant increase in cellular reactive oxygen species (measured by using the probe DCDCDHF) was observed after treatment with 50 μM Fe^{2+} both by fluorescence microscopy and spectrofluorometry (Fig. 1, *D* and *E*). Moreover, synaptophysin, an integral membrane protein of synaptic vesicles whose distribution and abundance make it a useful synaptic marker, was observed to be decreased significantly after the exposure to 50 μM Fe^{2+} (Fig. 1*F*). These results allow us to define a model of mild oxidative stress-triggered neurodegeneration generated by the exposure of hippocampal HT22 neurons to 50 μM Fe^{2+}, characterized by noticeable morphological changes, increased production of cellular oxidants, and, thus, lipid peroxidation and a significant loss of synaptic endings, but without clear signs of neuronal death.

State of Akt and GSK3β Phosphorylation upon Fe^{2+}-induced Oxidative Stress—After characterizing our model, we next investigated the participation of the PI3K/Akt/GSK3β pathway in cellular signaling events triggered by iron-induced mild oxidative stress. Akt and GSK3β phosphorylation levels were evaluated by Western blot analysis and normalized to total Akt and GSK3β levels, respectively. Consistent with our previous results in isolated synaptic endings (18, 19), the presence of iron (25 and 50 μM) caused an increase in the phosphorylation levels of both Akt (737 and 648% with respect to the control for 25 and 50 μM Fe^{2+}, respectively) and GSK3β (100 and 335% with respect to the control for 25 and 50 μM Fe^{2+}, respectively, Fig. 2*A*) in HT22 neurons. Of note, Akt is activated when phosphorylated in serine 473, whereas GSK3β is inhibited when phosphorylated in serine 9. The well documented PI3K inhibitor LY294002 (10 μM) strongly decreased Akt phosphorylation in the presence of iron. These results support the PI3K dependence of Akt activation under oxidative stress conditions in hippocampal neurons (Fig. 2*B*). Because these data support our

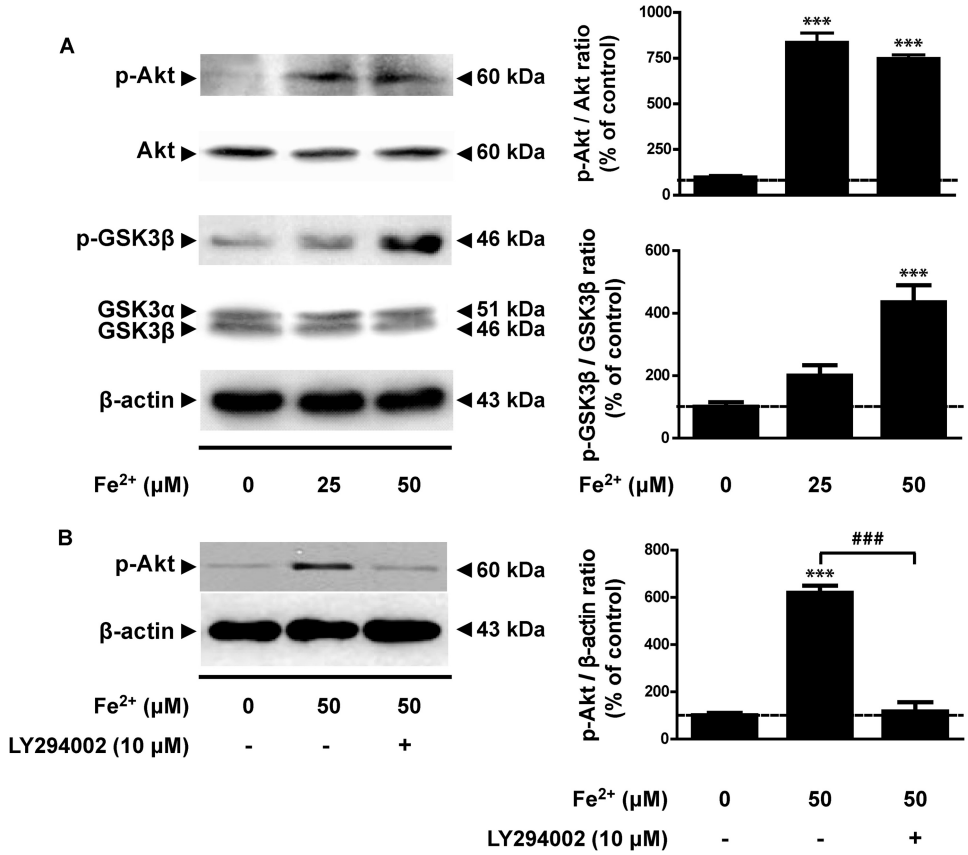

FIGURE 2. **Western blot analyses of the PI3K/Akt pathway.** *A*, cells were exposed to Fe^{2+} (25 and 50 μM) for 24 h. Cell lysates were prepared for Western blot analysis as described under "Experimental Procedures," and Akt and GSK3β phosphorylation was assessed. The Western blot in each case is representative of three different experiments. Bands of proteins were quantified using scanning densitometry. The data in the *graphs* in the *right panel* represent the ratio between the phosphorylated state and the total level of each protein, expressed as a percentage of the corresponding control condition (mean ± S.E. of three different experiments). ***, $p < 0.001$ for each condition with respect to the control; one-way ANOVA and Tukey's post hoc test. *B*, cells were incubated with 10 μM LY294002 or its vehicle for 30 min before exposure to Fe^{2+} and all along the treatment (24 h). Cell lysates were prepared for Western blot analysis as described under "Experimental Procedures," and Akt phosphorylation was assessed. The Western blot shown is representative of three different experiments. Proteins were quantified as indicated in *A*. The results are expressed as a percentage of the control (mean ± S.E. of three different experiments). ***, $p < 0.001$ with respect to the control; ###, $p < 0.001$ shown in the picture; one-way ANOVA and Tukey's post hoc test.

notion that this pathway, found previously to be activated locally in the synaptic terminals, is activated in the whole neuron, we hypothesize that the PI3K/Akt pathway plays a key role in the neuronal response to oxidative stress, participating either in pathogenic or protective mechanisms.

Role of PI3K/Akt/GSK3β in Iron-induced Cellular Oxidant Generation—To test our hypothesis that PI3K/Akt/GSK3β pathway is involved in some way in the generation of reactive oxygen species (ROS), cells were incubated with either 10 μM LY294002 or its vehicle for 30 min prior to the exposure to 50 μM Fe^{2+} (and then all along the treatment with this metal), and cellular oxidant levels were evaluated by fluorescence microscopy using the probe DCDCDHF. As shown in Fig. 3*A, 2*, ROS content increased after exposure to 50 μM Fe^{2+}. When cells were coincubated with LY294002, the increase in cellular oxidants was greater than that observed in the presence of iron alone (Fig. 3*A*, *3*). These results suggest that PI3K plays a protective role against oxidative stress, hindering the production of cellular oxidants.

To reinforce these results, cells were incubated with either 10 μM LY294002, 5 mM Li^+ (GSK3β inhibitor), 10 μM of inhibitor IV (Akt inhibitor), or the corresponding vehicles for 30 min prior to the exposure to 50 μM Fe^{2+} (and then all along the treatment with the latter), and cellular oxidant levels were measured by spectrofluorometry using DCDCDHF (Fig. 3*B*). The coincubation of iron and LY294002 (PI3K inhibition) caused a significant increase in ROS levels compared with incubation in the presence of iron alone. The same result was found with the coincubation of iron and inhibitor IV (Akt inhibition). No changes were observed after the coincubation of iron and Li^+ (GSK3β inhibition, which mimics the outcome of Akt activation).

To further address the role of Akt in the process of ROS generation during iron-induced oxidative stress, HT22 cells were transfected with either a constitutively active mutant of Akt (Myr-Akt) or the empty vector before the treatments with Fe^{2+} or its vehicle. As seen in Fig. 3*C*, overexpression of constitutively active Akt abolished Fe^{2+}-induced ROS generation. Taken together, these data allow us to conclude that both PI3K and its downstream effector Akt play crucial roles in preventing the increase of cellular oxidants in a model of mild oxidative insult. However, GSK3β either does not participate in ROS generation or has already been inhibited by Fe^{2+} and is not further inhibited by Li^+.

PI3K/Akt/GSK3β Intracellular Trafficking upon Oxidative Stress—Because Akt was shown to be phosphorylated (activated) after iron treatment, we sought to determine whether

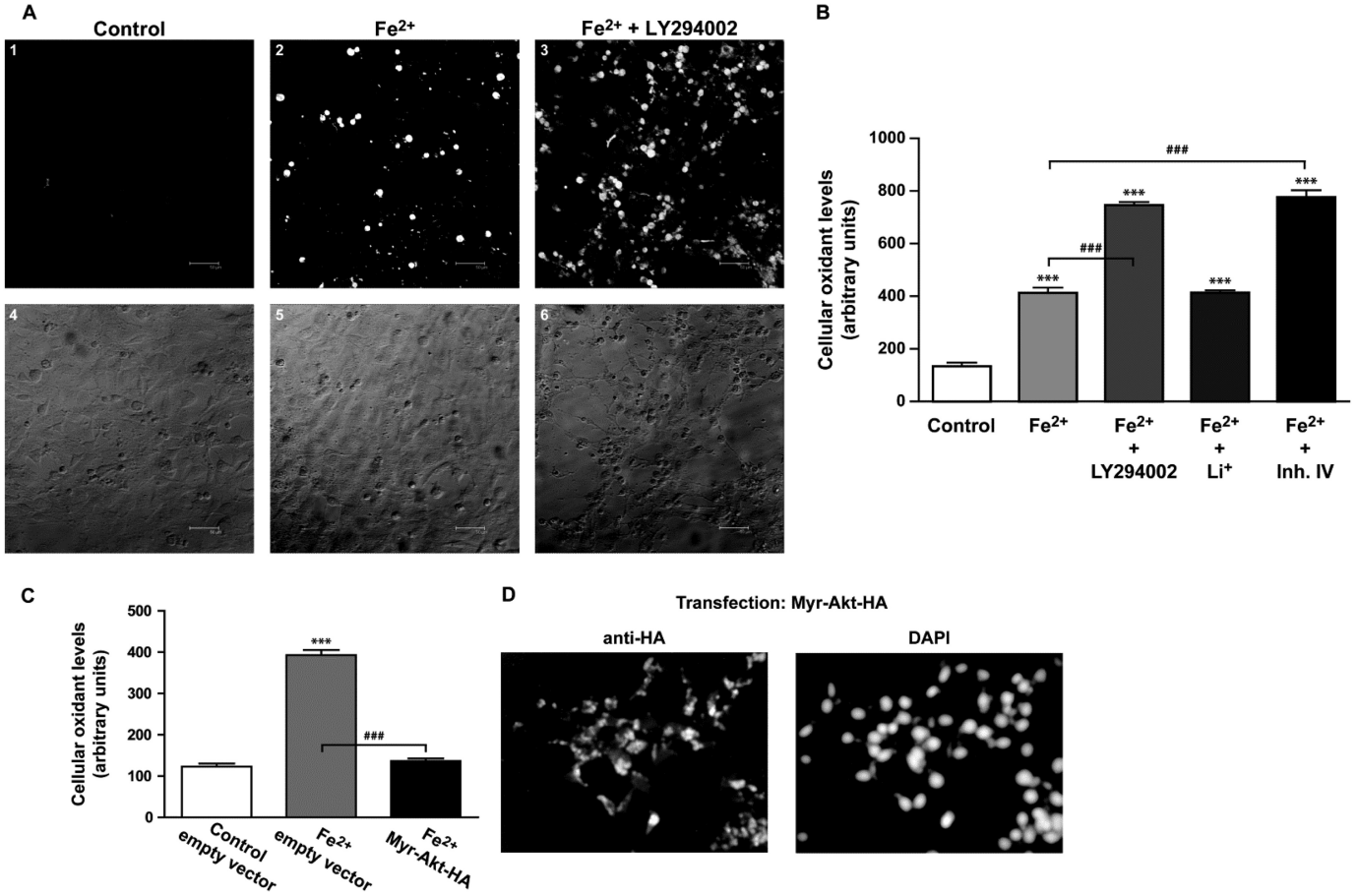

FIGURE 3. **Cellular oxidant production.** *A*, HT22 cells were incubated with 10 μM LY294002 or its vehicle for 30 min before exposure to Fe^{2+} and all along the treatment (24 h). They were subsequently incubated with 10 μM DCDCDHF for 30 min and imaged with an epifluorescence microscope (*1*, *2*, and *3*). *4*, *5*, and *6* show differential interference contrast images of *1*, *2*, and *3*, respectively. *B*, HT22 cells were treated with either 10 μM LY294002, 5 mM Li^+, 10 μM inhibitor IV, or their vehicles for 30 min before the addition of 50 μM Fe^{2+}. Cellular oxidant levels were quantified by spectrofluorometry. The results are expressed as arbitrary units and represent mean ± S.E. ($n = 3$–5). ***, $p < 0.001$ for each condition with respect to the control; ###, $p < 0.001$ shown in the picture; one-way ANOVA and Tukey's post hoc test. *C*, cells were transfected with either HA-Myr-Akt or the empty vector and subsequently exposed to 50 μM Fe^{2+}. Cellular oxidant levels were quantified as described previously. Results are expressed as arbitrary units and represent the mean ± S.E. ($n = 3$). ***, $p < 0.001$ with respect to the control; ###, $p < 0.001$ shown in the picture; one-way ANOVA and Tukey's post hoc test. *D*, cells were transfected with HA-Myr-Akt and processed for immunocytochemistry using antibodies against HA (*left panel*) to show transfection efficiency. DAPI was used as nuclear marker (*right panel*).

iron-induced PI3K/Akt activation involved a differential cellular compartmentalization or redistribution of its components. For this purpose, cells were treated with 50 μM Fe^{2+} for 24 h and then PI3K, Akt, GSK3β, and phosphatase and PTEN localization was assessed by immunocytochemistry (Fig. 4, *A*–*D*). Fluorescence microscopy studies show clearly that both PI3K and Akt increased their nuclear localization after treatment with the metal ion compared with the control condition (Fig. 4, *A* and *B*). However, GSK3β showed the opposite pattern. It decreased its nuclear localization in the presence of Fe^{2+} (Fig. 4*C*). PTEN was mainly located in the nucleus both in control and treated cells and did not show any significant change in response to iron treatment (Fig. 4*D*).

To further substantiate the results observed by immunocytochemistry, Fe^{2+}-treated cells were collected, and the nuclear and cytosolic fractions were isolated and analyzed by Western blot analysis. Human NAP-related protein and MAPK/ERK kinase were used as nuclear and cytosolic markers, respectively, and β-actin was used as a loading control. Both PI3K and Akt translocated to the nucleus after Fe^{2+}-triggered oxidative stress. GSK3β translocated from the nucleus to the cytosol, and PTEN showed no significant change (Fig. 4*E*). Together, these findings show that both PI3K and Akt undergo intracellular trafficking toward the nuclear compartment and that GSK3β is redirected in the opposite direction in response to iron-induced oxidative stress.

Consequences of Fe^{2+}-induced Oxidative Stress on FoxO3a Transcription Factor—Because PI3K/Akt translocated to the nucleus in response to oxidative stress and FoxO transcription factors are well known molecular targets of PI3K/Akt, we next investigated whether this pathway exerts any effects on FoxO3a. Subcellular fractionation followed by Western blot studies showed that phosphorylated Foxo3a (the transcriptionally inactive form) strongly increased in the cytosolic fraction (and, to a much lesser degree, in the nuclear fraction) upon iron exposure, whereas total FoxO3a (both active and inactive forms) decreased in the nuclear fraction (Fig. 5*A*). In agreement with these results, immunocytochemistry experiments showed that, in the absence of iron, FoxO3a is mainly located in the nucleus but that, upon iron-induced oxidative stress, it is localized more in the cytosol although still present in the nucleus (Fig. 5*D*).

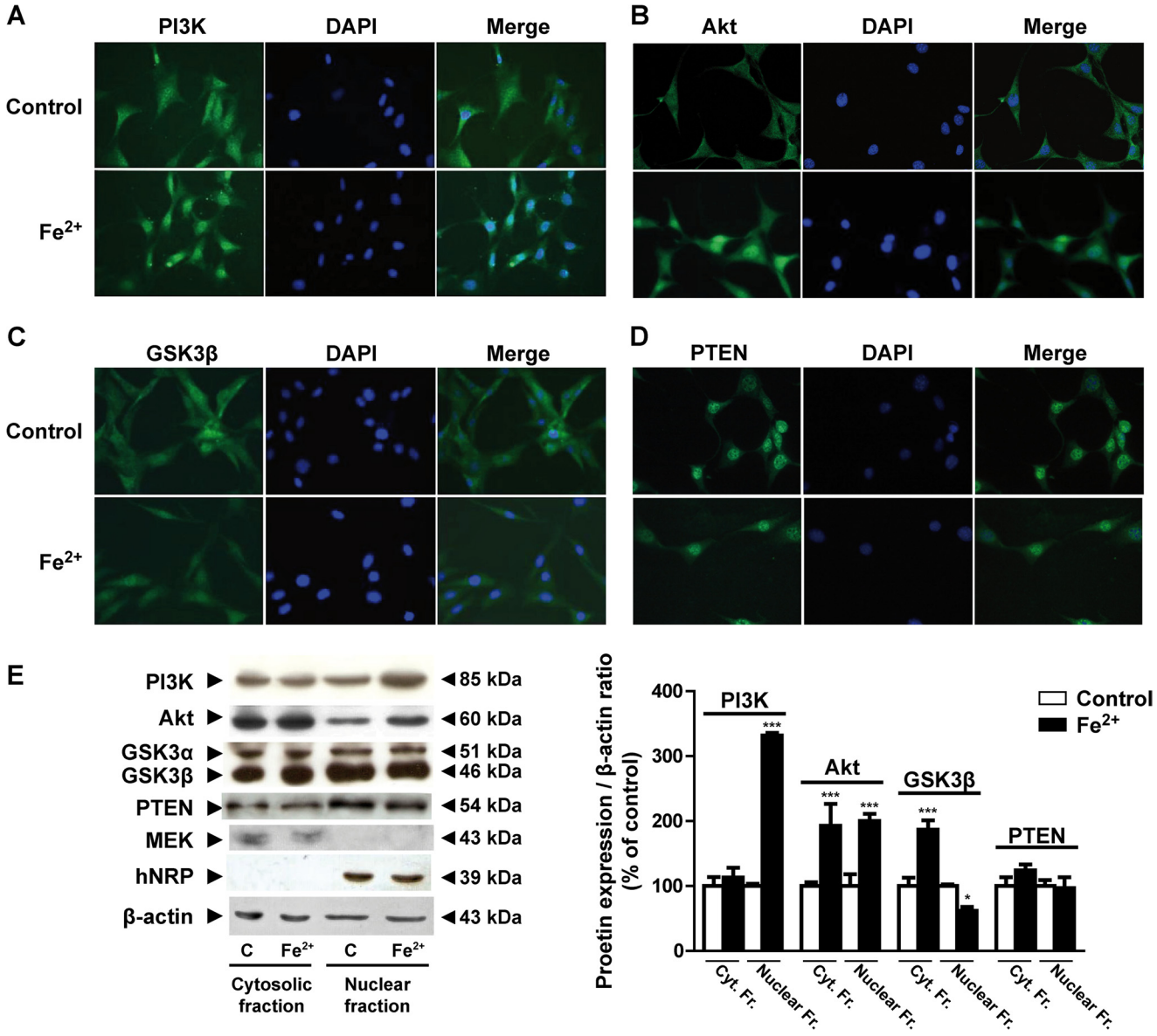

FIGURE 4. **Subcellular localization of the PI3K/Akt pathway.** (A-D) HT22 cells were grown onto coverslips, exposed to either 50 μM Fe^{2+} or its vehicle, and processed for immunocytochemistry using antibodies against PI3K (*A*), Akt (*B*), GSK3β (*C*), and PTEN (*D*). DAPI was used as nuclear marker in all the pictures (*A–D*). One representative picture from three different experiments is shown. *E*, subcellular fractions obtained from cells exposed to 50 μM Fe^{2+} (as described under "Experimental Procedures") were analyzed by Western blot analysis using antibodies against PI3K, Akt, GSK3β, and PTEN. MAPK/ERK kinase was used as cytosolic marker and human NAP-related protein as a nuclear marker. β-actin was used as a loading control. The blot in each case is representative of at least three different experiments. Bands of proteins were quantified using scanning densitometry. The data in the *graph* in the *right panel* represent the ratio between subcellular protein expression and β-actin, expressed as a percentage of the corresponding control condition (mean ± S.E. of three different experiments). *, $p < 0.05$; ***, $p < 0.001$ for each condition with respect to the control; one-way ANOVA and Tukey's post hoc test.

To correlate the increase in FoxO3a phosphorylation with PI3K/Akt activation, we carried out the same experiments in the presence of 10 μM LY294002. As shown in Fig. 5*B*, PI3K inhibition clearly abolished the increased phosphorylation of FoxO3a induced by Fe^{2+} in both the cytosolic and the nuclear fraction. Although it is generally accepted that Akt activation is a PI3K-dependent event, we also checked whether nuclear translocation of Akt was dependent on PI3K in our experimental model. Fig. 5*C* shows that incubation with LY294002 abolished the oxidative stress-induced translocation of Akt to the nucleus.

Because the antioxidant enzymes SOD1, SOD2, and catalase are well known target genes of FOXO3a transcriptional activity (24), their expression was assessed by Western blot analysis. Catalase showed no changes after the exposure to 50 μM Fe^{2+} with respect to the control, whereas SOD1 and SOD2 were found to be decreased under the same conditions (Fig. 5*E*).

Given that sirtuins (SirT) have been reported to participate in the regulation of FoxO transcription factors by acetylation, we investigated SirT3 subcellular distribution upon oxidative stress exposure. Western blot studies of cytosolic and nuclear fractions revealed that SirtT3 is localized mainly in the nucleus under the control condition and is exported out of the nucleus after iron treatment (Fig. 5*F*). Taken together, these results allow us to conclude that PI3K and Akt translocate to the nucleus in response to oxidative stress and that, consequently,

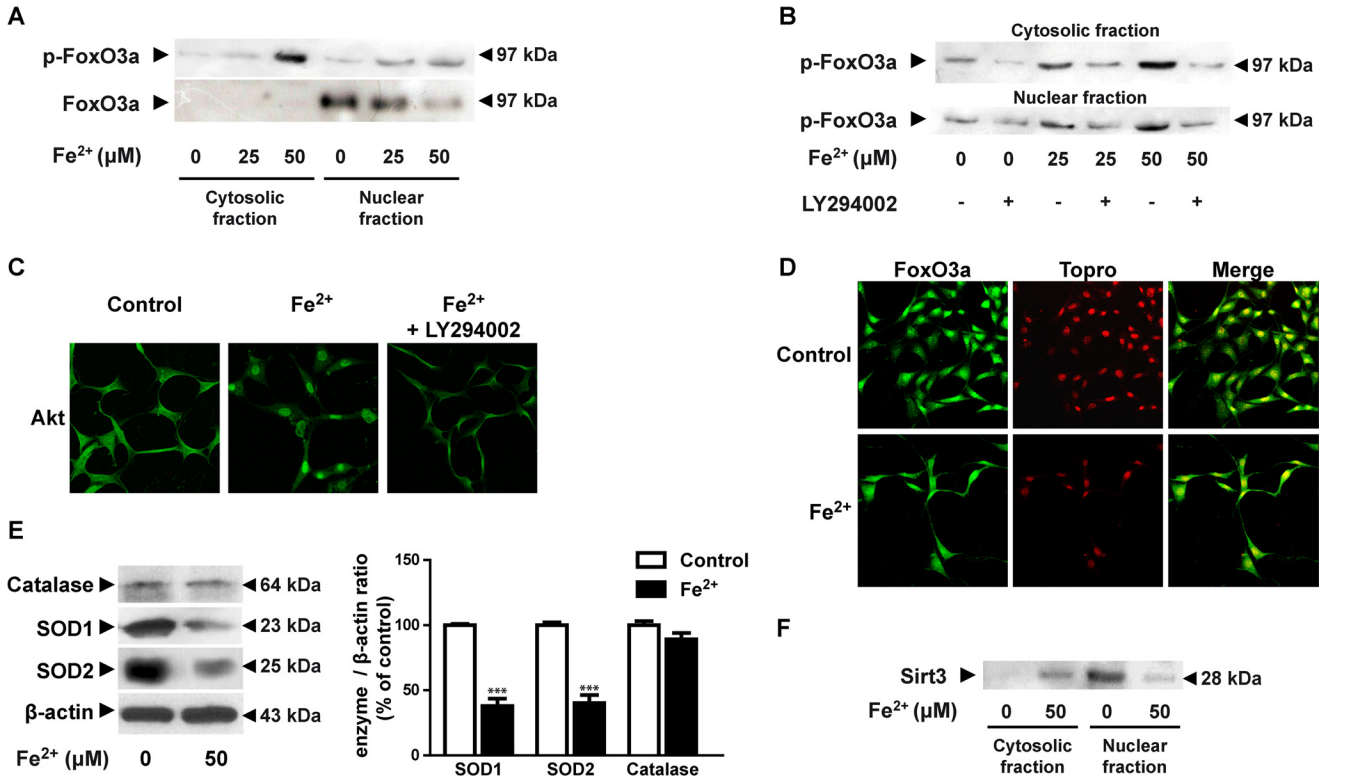

FIGURE 5. **FoxO3a trafficking.** *A*, subcellular fractions of HT22 cells exposed to either Fe^{2+} (25 and 50 μM) or its vehicle were analyzed by Western blot analysis using antibodies against phospho-FoxO3a and FoxO3a. The Western blot analysis shown is representative of at least three different experiments. *B*, subcellular fractions of HT22 cells incubated in the presence of 10 μM LY294002 (or its vehicle) and then exposed to either Fe^{2+} (25 and 50 μM) or its vehicle were analyzed by Western blot analysis using antibodies against phospho-FoxO3a. One representative blot of three different experiments is shown. *C*, cells were grown onto coverslips, incubated in the presence of 10 μM LY294002 (or its vehicle), exposed to either Fe^{2+} (25 and 50 μM) or its vehicle, and processed for immunocytochemistry using anti-Akt antibody. The picture shown is representative of three different experiments. *D*, cells were grown onto coverslips, exposed to either Fe^{2+} (25 and 50 μM) or its vehicle, and then processed for immunocytochemistry using anti-FoxO3a antibody. TO-PRO was used as nuclear marker. One representative picture of three different experiments is shown. *E*, lysates from cells exposed to either Fe^{2+} or its vehicle were studied by Western blot assays. The antibodies used were anti-SOD1, anti-SOD2, and anti-catalase. β-actin was used as a loading control. Each blot is representative of at least three different experiments. Bands of proteins were quantified using scanning densitometry. The data in the *graph* in the *right panel* represent the ratio between subcellular protein expression and β-actin, expressed as a percentage of the corresponding control condition (mean ± S.E. of three different experiments). ***, $p < 0.001$ for each condition with respect to the control; Student's *t* test. *F*, subcellular fractions of HT22 neurons exposed to either Fe^{2+} (50 μM) or its vehicle were analyzed by Western blot analysis using anti-sirtuin 3 antibody. The Western blot analysis shown is representative of at least three different experiments.

FoxO3a is phosphorylated in a PI3K-dependent manner and trafficked out of the nucleus to the cytosol. At the same time, SirT3 translocates from the nuclear compartment either to the cytosol or the mitochondrion in response to iron-triggered oxidative stress.

Role of PI3K/Akt in Neuronal Survival—Because PI3K/Akt was shown to be activated and, thus, involved in protecting against cellular oxidants upon Fe^{2+}-induced oxidative stress, we sought to determine whether activation of this pathway has any involvement in neuronal survival. For this purpose, cells were incubated in the presence of either Fe^{2+} or its vehicle or coincubated with 10 μM LY294002 and Fe^{2+}, and morphological changes, neuronal viability, and lipid peroxidation were assessed. Photomicrographs show that the presence of PI3K inhibitor together with Fe^{2+} exacerbates morphological alterations caused by Fe^{2+} alone (Fig. 6*A*). Similarly, MTT reduction showed that coincubation with LY294002 and Fe^{2+} strongly decreased neuronal survival compared with both the control and the Fe^{2+}-treated conditions (Fig. 6*B*). Intriguingly, the increase in lipid peroxidation levels observed during iron-induced oxidative stress did not change in the presence of LY294002 (Fig. 6*C*). To further investigate the role of Akt during oxidative stress, cells were transfected with either Myr-Akt (constitutively active mutant), the FoxO3a wild type (Foxo3a-WT), the FoxO3a triple mutant (FoxO3a-TM, phosphorylation-deficient mutant), or the empty vector and then treated with either Fe^{2+} or its vehicle. Cellular oxidant levels were evaluated in these cells using the probe DCDCDHF. Fig. 6*D* shows that there was no variation in neuronal oxidant levels under the control conditions irrespective of the protein that was overexpressed. Fe^{2+}-exposure increased the production of cellular oxidants in cells transfected with empty vectors. However, overexpression of Myr-Akt decreased Fe^{2+}-induced oxidants to the level of the control condition. Overexpression of FoxO3a-WT did not alter oxidant levels generated by Fe^{2+} itself, whereas overexpression of FoxO3a-TM significantly increased the production of neuronal oxidants generated by Fe^{2+}-exposure (Fig. 6*D*). As mentioned above, SOD1 and SOD2, well known target genes of FOXO3a (24), decreased upon iron-induced oxidative stress in our experimental model. Therefore, we sought to determine whether PI3K inhibition was able to restore the expression levels of these enzymes. Fig. 6*E* shows that the presence of LY294002 strongly increased SOD1 and SOD2 expression. GSH levels did not show signifi-

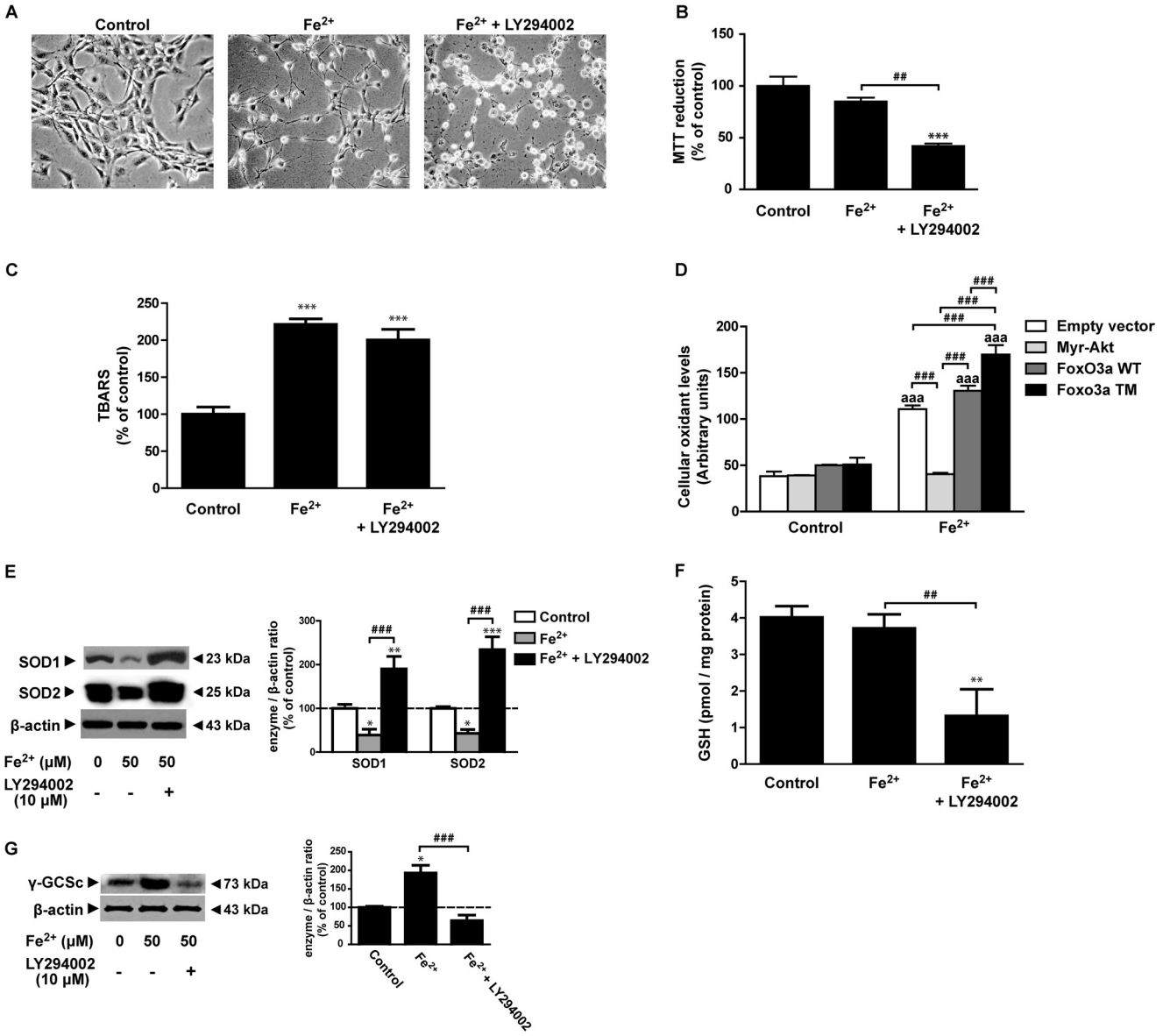

FIGURE 6. **Impact of PI3K inhibition on cell survival and ROS generation.** *A*, HT22 cells were incubated in the presence of 10 μM LY294002 (or its vehicle), exposed to either Fe^{2+} (50 μM) or its vehicle for 24 h, and then observed by bright-field microscopy. Photomicrographs are representative of three to four experiments. *B*, cells were treated as described in *A*, and cell viability was assessed by MTT reduction assay. The results are expressed as a percentage of the control and represent mean ± S.E. ($n = 3–4$). ***, $p < 0.001$ with respect to the control; ##, $p < 0.01$ as shown in the picture; one-way ANOVA and Tukey's post hoc test. *C*, cells were treated as described in *A*, and lipid peroxidation was quantified by TBARS assay. Results are expressed as a percentage of the control and represent mean ± S.E. ($n = 3–4$). ***, $p < 0.001$ with respect to the control; one-way ANOVA and Tukey's post hoc test. *D*, HT22 neurons were transfected with either Myr-Akt (constitutively active mutant), FoxO3a-WT (the wild-type form of FoxO3a), FoxO3a-TM (non-phosphorylable mutant), or the empty vector and exposed to Fe^{2+} for 24 h. Then cellular oxidant levels were evaluated using 10 μM DCDCDHF. Results (obtained by spectrofluorometry) are expressed as arbitrary units and represent mean ± S.E. ($n = 3–4$). aaa, $p < 0.001$ Fe^{2+}-treated condition with respect to the same overexpressed protein in the absence of the metal; ###, $p < 0.001$ as shown in the picture; two-way ANOVA and Tukey's post hoc test. *E*, lysates from cells treated as described in *A* were studied by Western blot assays. The antibodies used were anti-SOD1 and anti-SOD2. β-actin was used as a loading control. Each blot is representative of at least three different experiments. Bands of proteins were quantified using scanning densitometry. The data in the *graph* in the *right panel* represent the ratio between subcellular protein expression and β-actin, expressed as a percentage of the corresponding control condition (mean ± S.E. of three different experiments). *, $p < 0.05$; **, $p < 0.01$; and ***, $p < 0.001$ for each condition with respect to the control; ###, $p < 0.001$ shown in the picture; one-way ANOVA and Tukey's post hoc test. *F*, HT22 cells were treated as indicated in *A*, and GSH content was assessed. Results are expressed as pmol GSH/mg protein. **, $p < 0.01$ with respect to the control; ##, $p < 0.01$ shown in the picture; one-way ANOVA and Tukey's post hoc test. *G*, lysates from cells treated as described in *A* were analyzed by Western blot analysis. The antibody used was anti-γ-GCSc. β-Actin was used as a loading control. Each blot is representative of at least three different experiments. Bands of proteins were quantified as indicated in *E*. The data in the *graph* in the *right panel* represent the ratio between subcellular protein expression and β-actin, expressed as a percentage of the control (mean ± S.E. of three different experiments). *, $p < 0.05$ with respect to the control; ###, $p < 0.001$ shown in the picture; one-way ANOVA and Tukey's post hoc test.

cant changes in the presence of iron with respect to the control. However, the coincubation of iron with LY294002 strongly diminished GSH levels (Fig. 6*F*). For an additional explanation of this fact, we next examined the state of the γ-glutamylcysteine synthetase catalytic subunit (γ-GCSc), the rate-limiting step enzyme for GSH synthesis. In the presence of iron, γ-GCSc levels increased, and this rise in enzyme levels was abolished by LY294002 (Fig. 6*G*). These results led us to conclude that the

PI3K/Akt pathway plays a key role in neuronal survival by protecting cells from ROS generation through GSH metabolism regulation.

DISCUSSION

Oxidative stress has been considered as the main contributor to neuronal synaptic dysfunction and loss in AD (25–27). In line with this, compelling evidence has demonstrated that several neurodegenerative disorders involving oxidative stress are associated with an increase in brain Fe^{2+} levels during the onset and progression of the disease (28–31). Specifically, iron accumulation has been shown in brain regions with clear signs of neurodegeneration (32, 33). Recent studies have demonstrated that molecules with the ability to bind iron are effective in slowing disease progression in both AD models and patients. Indeed, it has also been observed that this metal ion progressively accumulates in the brain during normal aging (34). Over the last decade, our laboratory has made considerable progress in characterizing the effect of Fe^{2+} in different neuronal models, from the synaptic ending to the entire retina (18–20, 35–39). The PI3K/Akt/GSK3β signaling pathway has been of particular interest because it is involved in synaptic plasticity and neuronal survival (19). In this study, we have moved to a new neuronal model of Fe^{2+}-triggered mild oxidative stress. Under these conditions (50 μM Fe^{2+}), a pronounced loss of synaptic endings, increased generation of cellular oxidants and lipid peroxidation, but no marked signs of neuronal death, were observed. In addition, the PI3K/Akt pathway became activated together with the concomitant inhibition of one of its downstream targets, GSK3β. Our observations coincide with previous studies reporting that PI3K and its downstream effector Akt are activated in response to oxidative stress in neurons. The activation of this pathway in neurons subjected to oxidative injury has been largely associated with neuronal survival (40–42).

Our findings clearly illustrate that during Fe^{2+}-triggered mild oxidative stress in hippocampal neurons, Akt accumulates in the nucleus in a PI3K-dependent fashion and that this nuclear compartmentation of Akt gives rise to FoxO3a phosphorylation (a phenomenon also shown to be dependent on PI3K), inhibition, and nuclear exclusion. Of note, both Akt and PI3K increase their nuclear localization without involving cytosolic depletion, as would be expected. One possible explanation is that an increased expression of these proteins could occur to maintain their cytosolic concentration, thus counteracting depletion as a consequence of nuclear translocation. In this connection, similar patterns of subcellular distribution have been shown by Boehme *et al.* (43), Nguyen *et al.* (44), Badve *et al.* (45), and Ahn *et al.* (46) for Akt and by Dai *et al.* (47) for PI3K regulatory (p85) and catalytic (p110) subunits, respectively. Whether Akt-mediated phosphorylation of FoxO3a occurs in the cytosol (after nuclear exclusion) or in the nucleus remains to be clarified. In this regard, we consider that there is reasonable evidence to indicate that Akt catalyzes FoxO3a phosphorylation in the nucleus prior to transcription factor exclusion (48, 49). If, on the other hand, FoxO3a was phosphorylated in the cytosol, what would be the driving force that makes FoxO3a translocate to the cytosol before being phosphorylated? And why would Akt be trafficked to the nucleus after phosphorylating FoxO3a in the cytosol?

Here we present evidence of the existence of two pools of Akt: cytosolic Akt, which is activated after oxidative insult and then phosphorylates, thus inhibiting GSK3β, and nuclear Akt (encompassed by PI3K), which phosphorylates FoxO3a, inhibiting its transcriptional activity and promoting its nuclear exit. Taken together, two prolife signals are displayed by the cell: the inactivation of FoxO3a-dependent transcription and GSK3β nuclear exclusion (12, 24, 50–53).

Interestingly, Akt-dependent FoxO3a inactivation leads to a decrease in SOD1 and SOD2 expression with no changes in catalase expression, raising the question as to why it does so because these antioxidant enzymes play an important role in defeating oxidative stress. Previous reports from Linen *et al.* (54) showed decreased SOD2 expression as a FoxO3a-dependent event that rendered the experimental model more vulnerable to oxidative stress. One possible explanation is that this is the calculated risk involved in diminishing the FoxO3a-dependent expression of prodeath genes such as FasL (a well documented target of FoxO3a). If this is so, it is logical to assume that the neuron would adopt an alternative protective mechanism against oxidative injury. The brain is known to generate large amounts of ROS, and ~2–4% of the oxygen consumed by the mitochondria is diverted to produce superoxide (55). SOD converts superoxide to hydrogen peroxide, which is subsequently converted to water and O_2 by glutathione peroxidase or catalase (55). Alternatively, hydrogen peroxide can react with Fe^{2+} through the Fenton reaction to generate hydroxyl radicals. Taking into account that the presence of Fe^{2+} would accelerate the transformation of hydrogen peroxide to hydroxyl radicals, catalase activity appears to be non-essential. In consequence, the most appropriate candidate for clearing hydroxyl radicals becomes GSH (56). Moreover, the increase in superoxide can also be overcome non-enzymatically by the consumption of GSH (57). In line with this, we demonstrate that γ-GCSc expression increases in the presence of iron, which may be responsible for the maintenance in the levels of GSH under oxidative stress conditions, and that this preferential defeating pathway is dependent on PI3K/Akt activation because its inhibition strongly diminished not only GSH but also γ-GCSc expression levels. In view of the results presented here, it can be suggested that the activation of Akt during mild Fe^{2+}-induced oxidative stress in hippocampal neurons mediates FoxO3a inhibition with a consequent diminution in the expression of death-related genes. In spite of the resultant SOD1 and SOD2 diminished expression, PI3K/Akt pathway governs the final outcome by balancing GSH content.

In addition to phosphorylation, acetylation/deacetylation is another mechanism of regulation of FoxO transcription factors upon oxidative stress (24). Our results suggest that the exit of FoxO3a from the nucleus occurs via SirT3 export. The latter may enhance the nuclear acetylated/deacetylated FoxO3a ratio, therefore collaborating in the trafficking of this transcription factor. Another possibility is that the exit of SirT3 from the nucleus makes way for a FoxO3a-deacetylating enzyme in the cytosol, thus promoting the return of the transcription factor to

the nuclear compartment. Further studies are required to clarify this issue.

Although generally known to play a key role in metabolism and in survival responses to numerous stimuli, the activated PI3K/Akt pathway has also been reported to promote cell death or play a prodeath role (15, 58). In seeking to resolve this ambiguity, we used different approaches to demonstrate the protective role that the PI3K/Akt pathway exerts in preventing the increase of cellular oxidants in our experimental model. The overexpression of Akt (constitutively active mutant) was sufficient to prevent the increase in ROS levels generated by Fe^{2+} exposure. However, this role cannot be attributed to a specific subcellular localization of Akt because myristolation of its N terminus facilitates activation by promoting the association of Myr-Akt with the plasma membrane, which may reduce nuclear translocation and retain more activity in the membrane cytoplasmic compartments but does not unequivocally dismiss the possibility of nuclear localization (59). On the other hand, when Akt-mediated phosphorylation of FoxO3a is abolished (FoxO3a-TM), ROS generation increased significantly. All these findings clearly illustrate that Akt has a nuclear protective role with FoxO3a as a key target (60). Our results do not rule out the possibility of an important additional cytosolic role of Akt. More in-depth studies would be required to resolve this. Unraveling the target genes that are up/down-regulated as a result of Akt-mediated FoxO3a inactivation as well as the antioxidant system used mainly by the neuron will provide important tools for future therapeutic treatment of oxidative stress-related diseases.

Acknowledgments—We thank Dr. Alex Toker (Department of Pathology, Beth Israel Deaconess Medical Center, Harvard Medical School) for providing the plasmids used in this work.

REFERENCES

1. Berg, D., and Youdim, M. B. (2006) Role of iron in neurodegenerative disorders. *Top. Magn. Reson. Imaging* **17,** 5–17
2. Kell, D. B. (2010) Towards a unifying, systems biology understanding of large-scale cellular death and destruction caused by poorly liganded iron. Parkinson's, Huntington's, Alzheimer's, prions, bactericides, chemical toxicology and others as examples. *Arch. Toxicol.* **84,** 825–889
3. Toker, A. (2000) Protein kinases as mediators of phosphoinositide 3-kinase signaling. *Mol. Pharmacol.* **57,** 652–658
4. Toker, A. (2012) Achieving specificity in Akt signaling in cancer. *Adv. Biol. Regul.* **52,** 78–87
5. Vanhaesebroeck, B., and Alessi, D. R. (2000) The PI3K-PDK1 connection. More than just a road to PKB. *Biochem. J.* **346,** 561–576
6. Fan, C. D., Lum, M. A., Xu, C., Black, J. D., and Wang, X. (2013) Ubiquitin-dependent regulation of phospho-AKT dynamics by the ubiquitin E3 ligase, NEDD4–1, in the IGF-1 response. *J. Biol. Chem.* **288,** 1674–1684
7. Meijer, L., Flajolet, M., and Greengard, P. (2004) Pharmacological inhibitors of glycogen synthase kinase 3. *Trends Pharmacol. Sci.* **25,** 471–480
8. Lucas, J. J., Hernández, F., Gómez-Ramos, P., Morán, M. A., Hen, R., and Avila, J. (2001) Decreased nuclear β-catenin, tau hyperphosphorylation and neurodegeneration in GSK-3β conditional transgenic mice. *EMBO J.* **20,** 27–39
9. Ryder, J., Su, Y., and Ni, B. (2004) Akt/GSK3β serine/threonine kinases. Evidence for a signalling pathway mediated by familial Alzheimer's disease mutations. *Cell. Signal.* **16,** 187–200
10. Furuyama, T., Nakazawa, T., Nakano, I., and Mori, N. (2000) Identification of the differential distribution patterns of mRNAs and consensus binding sequences for mouse DAF-16 homologues. *Biochem. J.* **349,** 629–634
11. Nakae, J., Park, B. C., and Accili, D. (1999) Insulin stimulates phosphorylation of the forkhead transcription factor FKHR on serine 253 through a Wortmannin-sensitive pathway. *J. Biol. Chem.* **274,** 15982–15985
12. Brunet, A., Bonni, A., Zigmond, M. J., Lin, M. Z., Juo, P., Hu, L. S., Anderson, M. J., Arden, K. C., Blenis, J., and Greenberg, M. E. (1999) Akt promotes cell survival by phosphorylating and inhibiting a Forkhead transcription factor. *Cell* **96,** 857–868
13. Fukunaga, K., Ishigami, T., and Kawano, T. (2005) Transcriptional regulation of neuronal genes and its effect on neural functions: expression and function of forkhead transcription factors in neurons. *J. Pharmacol. Sci.* **98,** 205–211
14. Su, B., Liu, H., Wang, X., Chen, S. G., Siedlak, S. L., Kondo, E., Choi, R., Takeda, A., Castellani, R. J., Perry, G., Smith, M. A., Zhu, X., and Lee, H. G. (2009) Ectopic localization of FOXO3a protein in Lewy bodies in Lewy body dementia and Parkinson's disease. *Mol. Neurodegener.* **4,** 32
15. Nogueira, V., Park, Y., Chen, C. C., Xu, P. Z., Chen, M. L., Tonic, I., Unterman, T., and Hay, N. (2008) Akt determines replicative senescence and oxidative or oncogenic premature senescence and sensitizes cells to oxidative apoptosis. *Cancer Cell* **14,** 458–470
16. Los, M., Maddika, S., Erb, B., and Schulze-Osthoff, K. (2009) Switching Akt. From survival signaling to deadly response. *BioEssays* **31,** 492–495
17. Lu, Q., Zhai, Y., Cheng, Q., Liu, Y., Gao, X., Zhang, T., Wei, Y., Zhang, F., and Yin, X. (2013) The Akt-FoxO3a-manganese superoxide dismutase pathway is involved in the regulation of oxidative stress in diabetic nephropathy. *Exp. Physiol.* **98,** 934–945
18. Uranga, R. M., Mateos, M. V., Giusto, N. M., and Salvador, G. A. (2007) Activation of phosphoinositide-3 kinase/Akt pathway by FeSO4 in rat cerebral cortex synaptic endings. *J. Neurosci. Res.* **85,** 2924–2932
19. Uranga, R. M., Giusto, N. M., and Salvador, G. A. (2009) Iron-induced oxidative injury differentially regulates PI3K/Akt/GSK3β pathway in synaptic endings from adult and aged rats. *Toxicol. Sci.* **111,** 331–344
20. Uranga, R. M., Giusto, N. M., and Salvador, G. A. (2010) Effect of transition metals in synaptic damage induced by amyloid β peptide. *Neuroscience* **170,** 381–389
21. Osborn, L., Kunkel, S., and Nabel, G. J. (1989) Tumor necrosis factor α and interleukin 1 stimulate the human immunodeficiency virus enhancer by activation of the nuclear factor κ B. *Proc. Natl. Acad. Sci. U.S.A.* **86,** 2336–2340
22. Dignam, J. D., Lebovitz, R. M., and Roeder, R. G. (1983) Accurate transcription initiation by RNA polymerase II in a soluble extract from isolated mammalian nuclei. *Nucleic Acids Res.* **11,** 1475–1489
23. Bradford, M. M. (1976) A rapid and sensitive method for the quantitation of microgram quantities of protein utilizing the principle of protein-dye binding. *Anal. Biochem.* **72,** 248–254
24. Calnan, D. R., and Brunet, A. (2008) The FoxO code. *Oncogene* **27,** 2276–2288
25. Mancuso, C., Scapagini, G., Currò, D., Giuffrida Stella, A. M., De Marco, C., Butterfield, D. A., and Calabrese, V. (2007) Mitochondrial dysfunction, free radical generation and cellular stress response in neurodegenerative disorders. *Front. Biosci.* **12,** 1107–1123
26. Shi, Q., and Gibson, G. E. (2007) Oxidative stress and transcriptional regulation in Alzheimer disease. *Alzheimer Dis. Assoc. Disord.* **21,** 276–291
27. Joseph, J. A., Shukitt-Hale, B., Casadesus, G., and Fisher, D. (2005) Oxidative stress and inflammation in brain aging. Nutritional considerations. *Neurochem. Res.* **30,** 927–935
28. Ayton, S., Lei, P., and Bush, A. I. (2012) Metallostasis in Alzheimer disease. *Free Radic. Biol. Med.*, DOI 10.1016/j.freeradbiomed.2012.10.558
29. Farina, M., Avila, D. S., da Rocha, J. B., and Aschner, M. (2013) Metals, oxidative stress and neurodegeneration. A focus on iron, manganese and mercury. *Neurochem. Int.* **62,** 575–594
30. Schneider, S. A., Hardy, J., and Bhatia, K. P. (2009) Iron accumulation in syndromes of neurodegeneration with brain iron accumulation 1 and 2. Causative or consequential? *J. Neurol. Neurosurg. Psychiatry* **80,** 589–590
31. Schneider, S. A., and Bhatia, K. P. (2013) Excess iron harms the brain. The syndromes of neurodegeneration with brain iron accumulation (NBIA). *J. Neural Transm.* **120,** 695–703
32. Castellani, R. J., Moreira, P. I., Liu, G., Dobson, J., Perry, G., Smith, M. A.,

and Zhu, X. (2007) Iron. The redox-active center of oxidative stress in Alzheimer disease. *Neurochem. Res.* **32,** 1640–1645
33. Connor, J. R., and Benkovic, S. A. (1992) Iron regulation in the brain. Histochemical, biochemical, and molecular considerations. *Ann. Neurol.* **32,** S51-S61
34. Bartzokis, G., Tishler, T. A., Shin, I. S., Lu, P. H., and Cummings, J. L. (2004) Brain ferritin iron as a risk factor for age at onset in neurodegenerative diseases. *Ann. N.Y. Acad. Sci.* **1012,** 224–236
35. Mateos, M. V., Uranga, R. M., Salvador, G. A., and Giusto, N. M. (2008) Activation of phosphatidylcholine signalling during oxidative stress in synaptic endings. *Neurochem. Int.* **53,** 199–206
36. Mateos, M. V., Giusto, N. M., and Salvador, G. A. (2012) Distinctive roles of PLD signaling elicited by oxidative stress in synaptic endings from adult and aged rats. *Biochim. Biophys. Acta* **1823,** 2136–2148
37. Rodríguez Diez, G., Uranga, R. M., Mateos, M. V., Giusto, N. M., and Salvador, G. A. (2012) Differential participation of phospholipase A(2) isoforms during iron-induced retinal toxicity. Implications for age-related macular degeneration. *Neurochem. Int.* **61,** 749–758
38. Salvador, G. A., Uranga, R. M., and Giusto, N. M. (2010) Iron and mechanisms of neurotoxicity. *Int. J. Alzheimers Dis.* **2011,** 720658
39. Salvador, G. A. (2010) Iron in neuronal function and dysfunction. *Biofactors* **36,** 103–110
40. Choi, H., Park, H. H., Koh, S. H., Choi, N. Y., Yu, H. J., Park, J., Lee, Y. J., and Lee, K. Y. (2012) Coenzyme Q10 protects against amyloid β-induced neuronal cell death by inhibiting oxidative stress and activating the P13K pathway. *Neurotoxicology* **33,** 85–90
41. Lee, Y. J., Park, K. H., Park, H. H., Kim, Y. J., Lee, K. Y., Kim, S. H., and Koh, S. H. (2009) Cilnidipine mediates a neuroprotective effect by scavenging free radicals and activating the phosphatidylinositol 3-kinase pathway. *J. Neurochem.* **111,** 90–100
42. Wang, S., Chong, Z. Z., Shang, Y. C., and Maiese, K. (2012) Wnt1 inducible signaling pathway protein 1 (WISP1) blocks neurodegeneration through phosphoinositide 3 kinase/Akt1 and apoptotic mitochondrial signaling involving Bad, Bax, Bim, and Bcl-xL. *Curr. Neurovasc. Res.* **9,** 20–31
43. Boehme, K. A., Kulikov, R., and Blattner, C. (2008) p53 stabilization in response to DNA damage requires Akt/PKB and DNA-PK. *Proc. Natl. Acad. Sci. U.S.A.* **105,** 7785–7790
44. Xuan Nguyen, T. L., Choi, J. W., Lee, S. B., Ye, K., Woo, S. D., Lee, K. H., and Ahn, J. Y. (2006) Akt phosphorylation is essential for nuclear translocation and retention in NGF-stimulated PC12 cells. *Biochem. Biophys. Res. Commun.* **349,** 789–798
45. Badve, S., Collins, N. R., Bhat-Nakshatri, P., Turbin, D., Leung, S., Thorat, M., Dunn, S. E., Geistlinger, T. R., Carroll, J. S., Brown, M., Bose, S., Teitell, M. A., and Nakshatri, H. (2010) Subcellular localization of activated AKT in estrogen receptor- and progesterone receptor-expressing breast cancers. Potential clinical implications. *Am. J. Pathol.* **176,** 2139–2149
46. Ahn, J. Y., Liu, X., Liu, Z., Pereira, L., Cheng, D., Peng, J., Wade, P. A., Hamburger, A. W., and Ye, K. (2006) Nuclear Akt associates with PKC-phosphorylated Ebp1, preventing DNA fragmentation by inhibition of caspase-activated DNase. *EMBO J.* **25,** 2083–2095
47. Dai, Y., Wei, Z., Sephton, C. F., Zhang, D., Anderson, D. H., and Mousseau, D. D. (2007) Haloperidol induces the nuclear translocation of phosphatidylinositol 3′-kinase to disrupt Akt phosphorylation in PC12 cells. *J. Psychiatry Neurosci.* **32,** 323–330
48. Van Der Heide, L. P., Hoekman, M. F., and Smidt, M. P. (2004) The ins and outs of FoxO shuttling. Mechanisms of FoxO translocation and transcriptional regulation. *Biochem. J.* **380,** 297–309
49. Vogt, P. K., Jiang, H., and Aoki, M. (2005) Triple layer control. Phosphorylation, acetylation and ubiquitination of FOXO proteins. *Cell Cycle* **4,** 908–913
50. Bijur, G. N., and Jope, R. S. (2001) Proapoptotic stimuli induce nuclear accumulation of glycogen synthase kinase-3 β. *J. Biol. Chem.* **276,** 37436–37442
51. Brunet, A., Park, J., Tran, H., Hu, L. S., Hemmings, B. A., and Greenberg, M. E. (2001) Protein kinase SGK mediates survival signals by phosphorylating the forkhead transcription factor FKHRL1 (FOXO3a). *Mol. Cell. Biol.* **21,** 952–965
52. Meares, G. P., and Jope, R. S. (2007) Resolution of the nuclear localization mechanism of glycogen synthase kinase-3. Functional effects in apoptosis. *J. Biol. Chem.* **282,** 16989–17001
53. Medina, M., and Wandosell, F. (2011) Deconstructing GSK-3. The fine regulation of its activity. *Int. J. Alzheimers Dis.* **2011,** 479249
54. Lijnen, P. J., van Pelt, J. F., and Fagard, R. H. (2010) Downregulation of manganese superoxide dismutase by angiotensin II in cardiac fibroblasts of rats. Association with oxidative stress in myocardium. *Am. J. Hypertens.* **23,** 1128–1135
55. Chance, B., Sies, H., and Boveris, A. (1979) Hydroperoxide metabolism in mammalian organs. *Physiol. Rev.* **59,** 527–605
56. Dringen, R. (2000) Metabolism and functions of glutathione in brain. *Prog. Neurobiol.* **62,** 649–671
57. Aoyama, K., Watabe, M., and Nakaki, T. (2008) Regulation of neuronal glutathione synthesis. *J. Pharmacol. Sci.* **108,** 227–238
58. Winterbourn, C. C., and Metodiewa, D. (1994) The reaction of superoxide with reduced glutathione. *Arch. Biochem. Biophys.* **314,** 284–290
59. Min, Y. K., Lee, J. E., and Chung, K. C. (2007) Zinc induces cell death in immortalized embryonic hippocampal cells via activation of Akt-GSK-3β signaling. *Exp. Cell Res.* **313,** 312–321
60. Webster, K. A. (2004) Aktion in the nucleus. *Circ. Res.* **94,** 856–859